Supplemental Document

Biomedical Optics EXPRESS

Melanin concentration maps by label-free super-resolution photo-thermal imaging on melanoma biopsies: supplement

Margaux Bouzin,[1,5] Mario Marini,[1,5] Giuseppe Chirico,[1,2,6] Francesca Granucci,[3] Francesca Mingozzi,[3] Roberto Colombo,[4] Laura D'Alfonso,[1] Laura Sironi,[1] and Maddalena Collini[1,2,7]

[1]*Physics Department, Università degli Studi di Milano-Bicocca, Piazza della Scienza 3, 20126, Milano, Italy*
[2]*CNR Institute for Applied Science and Intelligent Systems, Via Campi Flegrei 34, 80078, Pozzuoli, Italy*
[3]*Biotechnology and Biosciences Department, Università degli Studi di Milano-Bicocca, Piazza della Scienza 2, 20126, Milano, Italy*
[4]*Department of Earth and Environmental Sciences, Università degli Studi di Milano-Bicocca, Piazza della Scienza 1, 20126, Milano, Italy*
[5]*Equal contribution*
[6]*giuseppe.chirico@unimib.it*
[7]*maddalena.collini@unimib.it*

Supplement DOI: https://doi.org/10.6084/m9.figshare.17013956

Parent Article DOI: https://doi.org/10.1364/BOE.445945

MELANIN CONCENTRATION MAPS BY LABEL-FREE SUPER-RESOLUTION PHOTO-THERMAL IMAGING ON MELANOMA BIOPSIES

MARGAUX BOUZIN,[1,#] MARIO MARINI,[1,#] GIUSEPPE CHIRICO,[1,2,*] FRANCESCA GRANUCCI,[3] FRANCESCA MINGOZZI,[3] ROBERTO COLOMBO,[4] LAURA D'ALFONSO,[1] LAURA SIRONI,[1] AND MADDALENA COLLINI[1,2,*]

[1]Physics Department, Università degli Studi di Milano-Bicocca, Piazza della Scienza 3, 20126, Milano, Italy
[2]CNR Institute for Applied Science and Intelligent Systems, Via Campi Flegrei 34, 80078, Pozzuoli, Italy
[3] Biotechnology and Biosciences Department, Università degli Studi di Milano-Bicocca, Piazza della Scienza 2, 20126, Milano, Italy
[4] Department of Earth and Environmental Sciences, Università degli Studi di Milano-Bicocca, Piazza della Scienza 1, 20126, Milano, Italy

[#] These authors contributed equally to this work
[*] giuseppe.chirico@unimib.it , [*] maddalena.collini@unimib.it

Supplemental Information

- **Figure S1**: Absence of photo-damage following super-resolution photo-thermal imaging
- **Figure S2**: Transmitted-light image of the B16 murine melanoma biopsy imaged in Fig.1
- **Figure S3**: Photo-thermal signal in B16 melanoma biopsies excised 7 and 14 days upon cells inoculation
- **Figure S4**: Super-resolution photo-thermal image at increased laser activation time
- **Figure S5**: Finite-element numerical simulations – approximation to a single-layer sample
- **Figure S6**: Finite-element numerical simulations – negligible convective and radiative losses
- **Figure S7**: Schematic of the photo-thermal imaging setup

Figure S1: Absence of photo-damage following super-resolution photo-thermal imaging

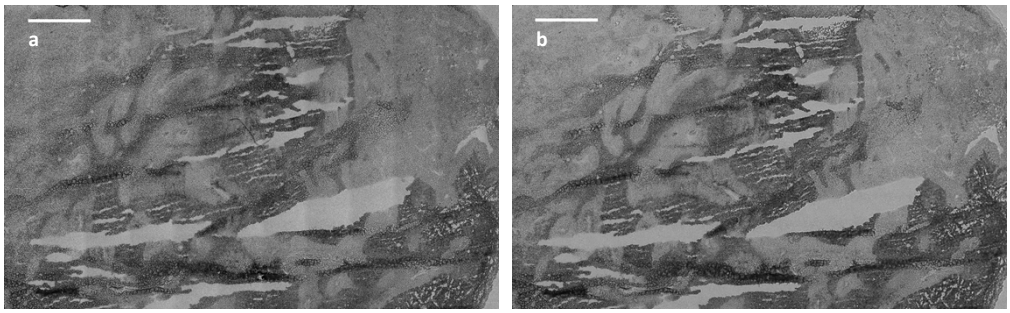

Figure S1. (a,b) Transmitted-light images of the same portion of a B16 murine melanoma biopsy before and right after the acquisition of the corresponding super-resolution photo-thermal image. The 33-mW laser power employed for the photo-thermal imaging experiment does not produce any evident photo-damage on the tissue section. A similar conclusion can be drawn for an analogous biopsy based on Figure 1b (main text) and Figure S2; the sample morphology in the h&e-stained section (Figure 1b) perfectly resembles the morphology of the same sample in the transmitted-light image of Figure S2: provided transmitted-light imaging and the h&e staining have been performed before and after photo-thermal imaging, respectively, this allows excluding thermography-related sample damage. Scale bars=1 mm.

Figure S2: Transmitted-light image of the B16 murine melanoma biopsy imaged in Fig.1

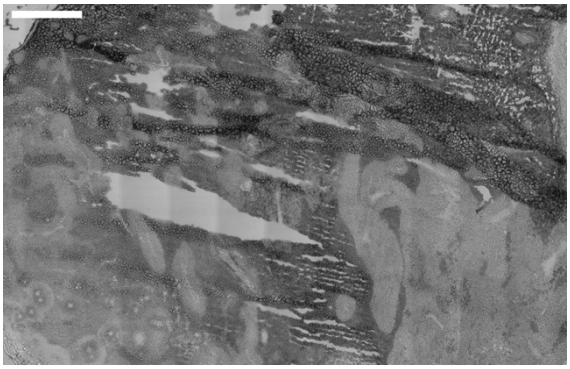

Figure S2. Transmitted-light image of a B16 murine melanoma biopsy. The comparison with the super-resolution thermal image of the same region (Figure 1a in the main text) confirms accurate reconstruction of the sample morphology by super-resolved thermography, and qualitatively highlights that the regions exhibiting more intense heat release are associated to lower light transmission, as expected in the presence of higher pigmentation. Scale bar=1 mm.

Figure S3: Photo-thermal signal in B16 melanoma biopsies excised 7 and 14 days upon cells inoculation

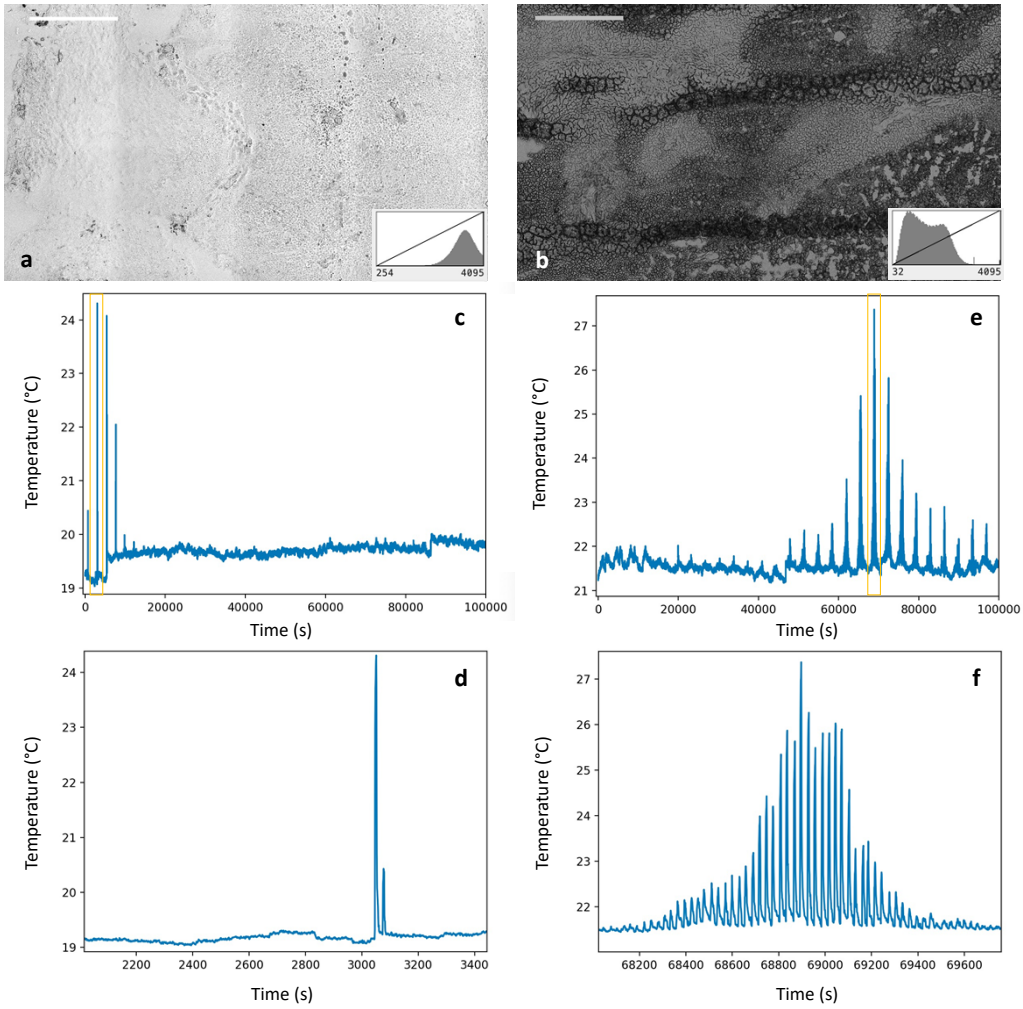

Figure S3. (a,b) Transmitted-light images of murine melanoma biopsies excised 7 (a) and 14 (b) days upon B16 cells inoculation in the mouse flank. Higher transmitted-light intensities in (a) are associated to a significantly lower pigmentation of the 7-day biopsy relatively to the 14-day one. Insets: histograms of intensity counts in arbitrary units. (c) Temperature time-trace extracted from an exemplary thermal camera pixel during super-resolution photo-thermal imaging on the tissue section shown in (a). (e) Temperature time-trace extracted from an exemplary thermal camera pixel during super-resolution photo-thermal imaging on the tissue section shown in (b). (d,f) Magnification of the yellow-boxed regions from panels (c) and (e), respectively. Each peak in the temperature time traces identifies a heat-release event primed by laser light absorption in the sample: temperature time profiles (c,e) and the corresponding magnifications in (d,f) highlight therefore a nearly-absent photo-thermal signal in the 7-day biopsy and a much more abundant photo-thermal signal in the more pigmented 14-day biopsy.

Figure S4: Super-resolution photo-thermal image at increased laser activation time

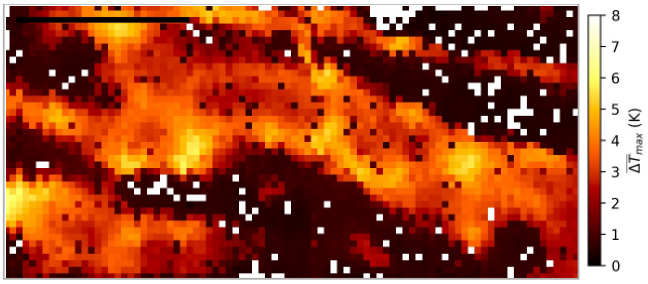

Figure S4. Super-resolved photo-thermal image of the region identified as ROI 3 in Figure 1a of the main text at increased laser activation time $\tau_{on} = 600$ ms. Acquisition parameters: $\lambda_{exc} = 514$ nm, $P_0 = 33$ mW, laser 1/e^2 radius $\omega = (28 \pm 1)$ µm, pixel size $\delta x = 37.8$ µm as in Figure 1a in the main text. Scale bar=1 mm. The histogram of the $\overline{\Delta T}_{max}$ amplitudes is reported in Figure 1e in the main text.

Figure S5: Finite-element numerical simulations – approximation to a single-layer sample

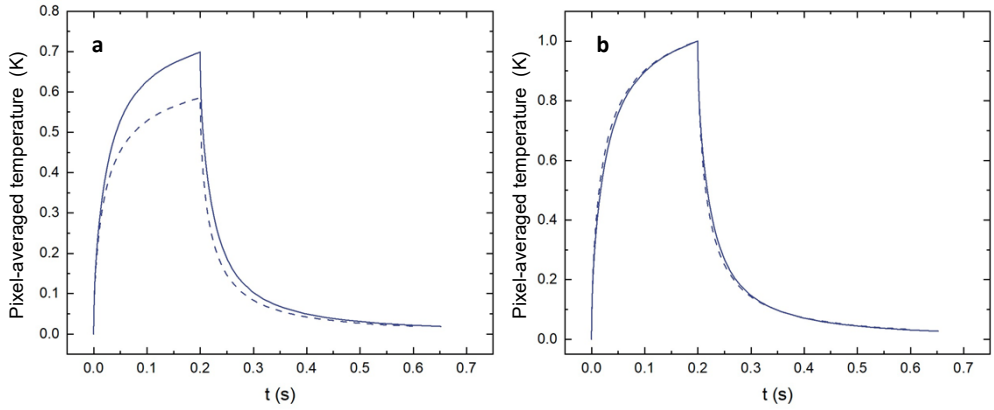

Figure S5. (a) Dashed blue line: temporal evolution of the amplitude of the temperature increment primed by a laser pulse with beam waist $\omega = 30$ µm and duration $\tau_{on} = 200$ ms on a 1020-µm thick glass slide (thermal conductivity k=0.9 $\mathrm{Wm^{-1}K^{-1}}$, thermal diffusivity $D = 5.02 \cdot 10^{-7}\mathrm{m^2s^{-1}}$; 0.5-mW absorbed laser power). Continuous blue line: temporal evolution of the amplitude of the temperature increment primed by a laser pulse with beam waist $\omega = 30$ µm and duration $\tau_{on} = 200$ ms on a two-layer material composed of a 20-µm thick tissue section (skin tissue, k=0.37 $\mathrm{Wm^{-1}K^{-1}}$, $D = 9.84 \cdot 10^{-8}\mathrm{m^2s^{-1}}$, 0.5-mW absorbed laser power) overlaid to a 1-mm thick glass slide (k=0.9 $\mathrm{Wm^{-1}K^{-1}}$, $D = 5.02 \cdot 10^{-7}\mathrm{m^2s^{-1}}$). (b) Normalization to unity of the profiles in (a). When compared to the case of a single-layer glass substrate, at identical absorbed laser power, the lower thermal conductivity of the 20-µm tissue layer increases the amplitude of the laser-primed temperature increment (panel a); the temporal kinetics of temperature evolution is unchanged instead (panel b). Therefore, an

identical temperature change and temporal evolution can in principle be obtained on the single-layer 1020-μm thick glass sample and on the double-layer glass+tissue sample provided the glass slide is subject to an increased effective laser power P_{eff}. Given the linear proportionality of the amplitude of temperature peaks to the excitation laser power, from the ratio of the temperature profiles in panel (a) we retrieve $P_{eff} = 1.2 \cdot P_0$, where P_0 denotes the laser power employed in the presence of the skin tissue section. Experimentally, it is therefore reasonable to assume that the overall heat transfer propagation in the imaged biopsies is dominated by the contribution of the underlying glass substrate (as intuitive based on the difference between the 1-mm and the 20-μm thicknesses), while light absorption and heat release are only determined by the absorbance A of the 20-μm tissue layer (no light absorption and heat release are observed for a single-layer 1-mm thick glass slide at the adopted incident 33-mW laser power). We model therefore each biopsy sample as a 1020-μm thick glass slide subject to a laser power P_{eff}. Temperature profiles have been simulated by finite-element numerical simulations on COMSOL Multiphysics (COMSOL AB, Stockholm, Sweden); k and D values for both skin and Corning glass have been derived from the COMSOL Material Library. The spatial average of temperature profiles over a square pixel size has been implemented in the simulation program (pixel size d=420 μm, as in the experimental conditions of the present work). Convective and radiative heat losses have been implemented with emissivity $\varepsilon = 0.9$ and a convective heat transfer coefficient $h = 10\ \mathrm{Wm^{-1}K^{-1}}$.

Figure S6: Finite-element numerical simulations – negligible convective and radiative losses

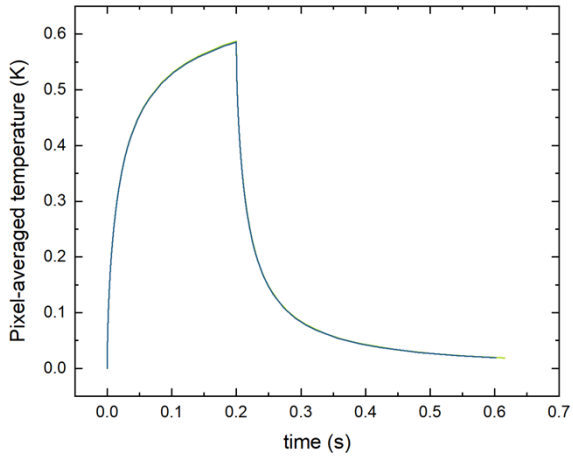

Figure S6. Comparison of the temporal profiles of the amplitude of the temperature increment primed by a laser pulse with beam waist $\omega = 30\ \mu\mathrm{m}$ and duration $\tau_{on} = 200\ \mathrm{ms}$ on a 1020-μm thick glass slide ($\mathrm{k} = 0.9\ \mathrm{Wm^{-1}K^{-1}}$, $D = 5.02 \cdot 10^{-7}\mathrm{m^2s^{-1}}$, 0.5-mW absorbed laser power) in the presence of radiative and convective heat losses (blue; emissivity $\varepsilon = 0.9$ and convective heat transfer coefficient $h = 10\ \mathrm{Wm^{-1}K^{-1}}$), and in the absence of heat losses (green). Temperature profiles have been simulated by finite-element numerical simulations on COMSOL Multiphysics (COMSOL AB, Stockholm, Sweden); the spatial average of temperature profiles over a square pixel size has been implemented in the simulation program (pixel size d=420 μm, as in the experimental conditions of the present work).

Figure S7: Schematic of the photo-thermal imaging setup

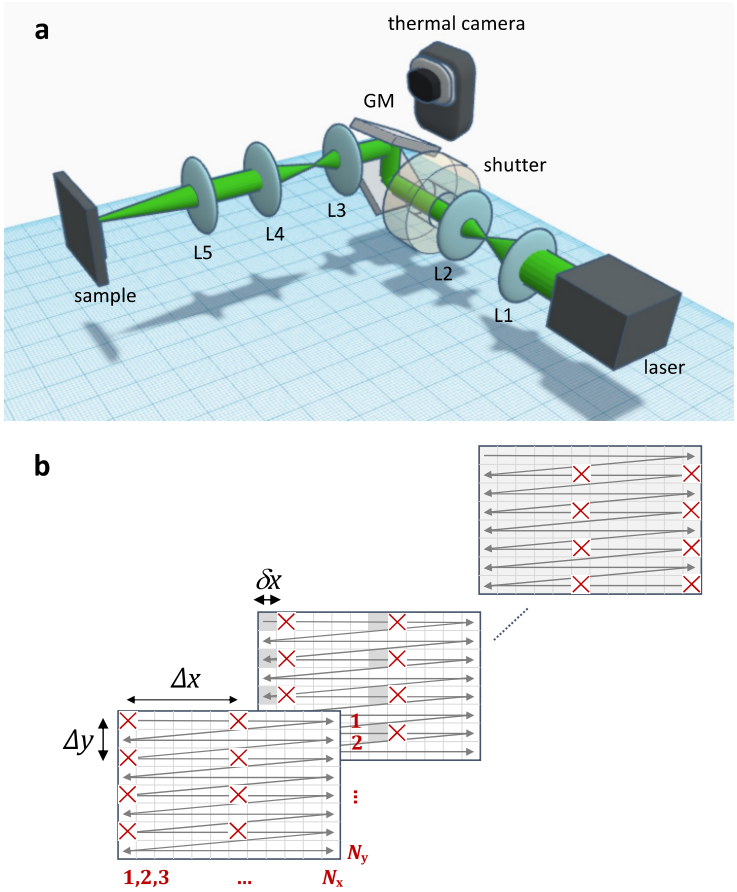

Figure S7. (a) Schematic of the setup employed for super-resolution photo-activated thermal imaging (L1-L5, lenses; GM, galvanometric mirrors). The detection of thermal radiation is performed by a thermal camera (FLIR T650sc, FLIR Systems Inc., OR, USA) in reflection mode (the thermal radiation is collected from the sample front face). (b) Schematic of the adopted raster-scanning modulated illumination scheme, depicted here with the first, second and last scans (from left to right) of an exemplary acquisition. The laser beam is scanned along a conventional raster path (grey arrows) with image format N_xxN_y and pixel size δx. During a single complete raster scan, laser illumination is only allowed (the shutter is only opened) on a limited set of isolated pixels (red crosses; grey pixels in each panel are those that have been illuminated during previous scans, whereas white pixels are those still to be illuminated by the laser beam). Δx defines the minimum distance (in pixel units) between two consecutively illuminated pixels along the x-direction, while Δy defines the distance between the nearest lines where the shutter can be opened (for convenience sake, values for Δx and Δy are chosen among the divisors of N_x and N_y, respectively). The raster scan must be repeated $\Delta x \Delta y$ times, with shifted sets of illuminated pixels, in order to illuminate the entire grid at least once. With laser pixel dwell times τ_{on} and τ_{off} during laser activation and de-activation, respectively, the time

required to scan the raster path once is $t_{\mathrm{scan}} = N_{\mathrm{x}}N_{\mathrm{y}}\tau_{\mathrm{on}}/(\Delta x\Delta y) + N_{\mathrm{x}}N_{\mathrm{y}}\tau_{\mathrm{off}}[1 - 1/(\Delta x\Delta y)]$. The total data acquisition time is therefore $t_{\mathrm{tot}} = t_{\mathrm{scan}}\Delta x\Delta y$.